analytical chemistry

Editors' Highlight

pubs.acs.org/ac

From Protein Complexes to Subunit Backbone Fragments: A Multi-stage Approach to Native Mass Spectrometry

Mikhail E. Belov,[†,§] Eugen Damoc,[†] Eduard Denisov,[†] Philip D. Compton,[‡] Stevan Horning,[†] Alexander A. Makarov,*[,†] and Neil L. Kelleher*[,‡]

[†]Thermo Fisher Scientific, 28199 Bremen, Germany

[‡]Northwestern University, Evanston, Illinois 60208, United States

Supporting Information

ABSTRACT: Native mass spectrometry (MS) is becoming an important integral part of structural proteomics and system biology research. The approach holds great promise for elucidating higher levels of protein structure: from primary to quaternary. This requires the most efficient use of tandem MS, which is the cornerstone of MS-based approaches. In this work, we advance a two-step fragmentation approach, or (pseudo)-MS^3, from native protein complexes to a set of constituent fragment ions. Using an efficient desolvation approach and quadrupole selection in the extended mass-to-charge (m/z) range, we have accomplished sequential dissociation of large protein complexes, such as phosporylase B (194 kDa), pyruvate kinase (232 kDa), and GroEL (801 kDa), to highly charged monomers which were then dissociated to a set of multiply charged fragmentation products. Fragment ion signals were acquired with a high resolution, high mass accuracy Orbitrap instrument that enabled highly confident identifications of the precursor monomer subunits. The developed approach is expected to enable characterization of stoichiometry and composition of endogenous native protein complexes at an unprecedented level of detail.

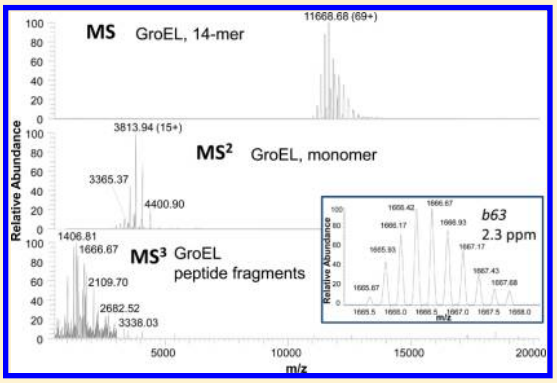

A variety of functional modules in biological systems are higher-order protein complexes. They often act as molecular machineries or information processing hubs in cellular networks.[1−4] Since its introduction in the early 1990s,[5−7] mass spectrometry (MS) of native protein complexes ionized from physiological buffers, also referred to as "native" MS, has become a robust and integral part of proteomics and systems biology.[8−14] In combination with X-ray crystallography,[15,16] solution and solid-state NMR,[17−19] small-angle X-ray scattering,[20,21] and electron microscopy,[22] native MS provides important complementary information on structure, topology, and architecture of protein complexes. The most common approach for preserving noncovalent interactions and transferring a protein complex from aqueous solution into the gas phase is nano electrospray ionization (nESI).[23] Under optimized conditions, nESI is capable of stabilizing, although transiently, the native structures of protein complexes by forming electrostatic interactions on protein surfaces.[24]

A landscape-changing development in the analysis of native protein complexes was the coupling of low-field ion mobility spectrometry (IMS) and MS.[25−28] These advances demonstrated that native topologies and quaternary structures of protein complexes could be preserved in the gas phase in the absence of bulk water, while IMS at a reduced pressure could elucidate shapes and collisional cross sections of heterogeneous macromolecular assemblies. To date, all native IMS-MS studies were carried out with different generations of Synapt HDMS instruments (Waters, Manchester, U.K.), which encompass a traveling wave ion guide (TWIG) followed up by an orthogonal acceleration time-of-flight mass spectrometer (OTOF MS).[29,30] Despite enabling structural insights into protein assemblies, the current IMS-MS approach has certain constraints for large protein complexes (>500 kDa), such as a limited pool of calibrant ions and lower IMS resolution of 10−15.[31]

In conjunction with scanning transmission electron microscopy (STEM) and atomic force microscopy (AFM), nESI-MS approaches have also been applied to determination of stoichiometry and composition of intact viruses and capsids. Molecular masses of ≈3 MDa and ≈4 MDa capsids, as well as dissociated counter complexes and ejected monomers and dimers, were measured with an accuracy of 0.1%.[32] Native MS has also been successfully employed for detection of intact heteromeric membrane protein complexes formed by polar cytoplasmic and nonpolar transmembrane subunits. It was shown that by maintaining detergent micelles in solutions well above the critical micelle concentration, interactions between cytoplasmic and transmembrane subunits were protected and the intact protein complexes could be then released through gas-phase activation.[33] Yet another remarkable advance has been detection of large (>700 kDa) intact protein complexes

Received: September 14, 2013
Accepted: November 15, 2013

   dx.doi.org/10.1021/ac4029328 | *Anal. Chem.* XXXX, XXX, XXX−XXX

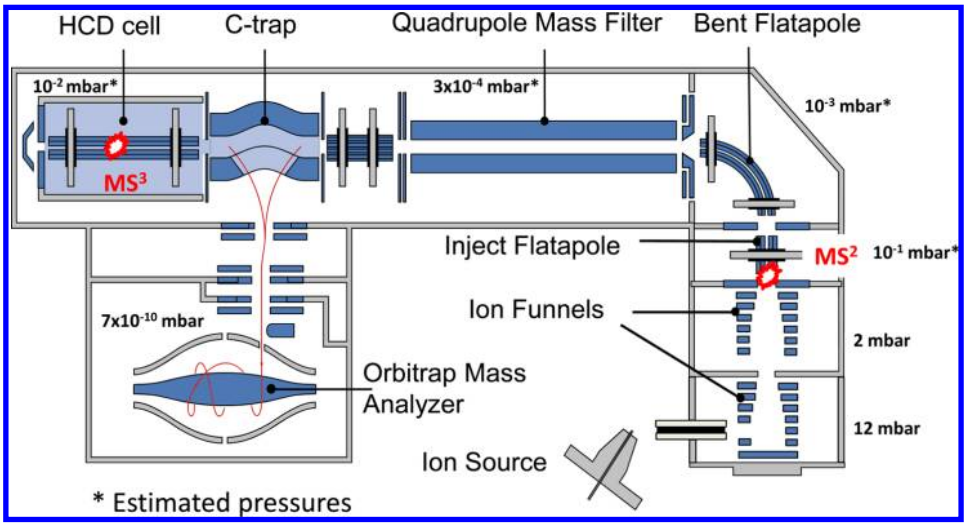

Figure 1. Schematic diagram of the modified Q Exactive mass spectrometer. The instrument encompasses a dual-funnel interface with orthogonal ion injection and quadrupole mass filter operating at a reduced rf-frequency of 285 kHz. Inject and bent flatapoles rf frequencies have been reduced to 2.6 MHz to improve higher m/z transmission.

with an Orbitrap mass spectrometer.[34] Rose et al. have shown that large protein complexes could be detected with sensitivity approaching single ions at high mass resolution.

While all the above developments have asserted the role of native MS as an integral part of structural proteomics and systems biology, the long-term challenge is to extend technology and methodology to operate across all levels of protein structure, from the quaternary to the primary. This will require the efficient use of tandem MS, the cornerstone of MS-based approaches, across a wide range of mass-to-charge ratios (m/z). The latter implies the capability of dissociating protein complexes into monomers (e.g., by ejecting highly charged monomer subunits from a heteromeric complex using different activation approaches, including collision induced dissociation, CID), selecting a specific type of monomer ions by their m/z (e.g., with a quadrupole mass analyzer), fragmenting the selected monomers to a set of constituent fragment ions (e.g., in a dedicated collision cell using higher energy CID), and detecting multiply charged fragment ions at high mass resolution and mass measurement accuracy (e.g., with a high resolution mass spectrometer). This fragmentation pathway would result in high confidence identification of the complex-encompassing monomer subunits and will concomitantly determine stoichiometry and composition of the intact protein complex. Furthermore, the two-step fragmentation pathway (or MS^3) would need to be made robust and applicable to high throughput studies of endogenous protein complexes from sub cellular fractions or organelles, similar to MS^2 employed in high throughput "top-down" proteomic approaches.[35] Despite remarkable technological advances in native MS, the aforementioned fragmentation pathway is not yet available for protein complexes, as briefly described below.

In a typical CID experiment, a protein complex will undergo thousands of collisions with neutral inert gas molecules, thereby converting its energy from kinetic to internal modes. Gradually accumulated internal energy would distribute to numerous degrees of freedom and partially dissipate to the environment.[36,37] When collisionally activated, a protein complex would go through a cascade of events, depending on the available internal energy: cleaning, restructuring, unfolding, dissociation, and fragmentation. Using the IMS-MS approach with Acr1, a 197-kDa heat shock protein from *Mycobacterium tuberculosis* composed of identical subunits arranged as a hollow tetrahedron, Benesch[38] has shown that collision-induced restructuring may result in collapsing of the ring topology into globular forms, so that the collisional cross-section of the Acr1 protein complex, which assumes a dodecamer structure, would initially decrease upon gentle collisional activation. With a further increase in the collision energy, a conformational change into an unfolded structure occurred and the collisional cross-section was found to increase, which the result is ascribed as protein complex unfolding. At the maximum available activation energy, the Acr1 complex dissociated into counter complexes, such as undecamers and decamers, and highly charged monomers. Only a few singly charged fragment ions were observed at unreported mass accuracy that was inadequate to identify the monomers.

Similarly, releasing more than two subunits from 67+ ion of tetradecameric GroEL chaperonin has been found intractable,[39] even after supercharging the complex by adding m-nitrobenzyl alcohol (m-NBA) to the spray solution and shifting the average charge from 66+ to 71+.[40] It was later reported that when the first and second monomers leave a GroEL complex, they carry away 14% of the mass and 70% of the charge, and dissociation of a third monomer was simply impossible because the number of residual charges was insufficient.[41] This means that the majority of the complex, that is often the core of the assembly, could not be studied via this approach, and alternative methods would need to be embraced to fully characterize the topology of macromolecular assemblies.

The use of electron capture dissociation (ECD) has been also explored in conjunction with native MS applications. One set of experiments was performed with a 12 T Fourier transform ion cyclotron resonance (FTICR) mass spectrometer using a 147 kDa yeast alcohol dehydrogenase (ADH) tetramer complex.[42] While efficiently breaking covalent bonds of larger proteins, ECD is known to preserve noncovalent interactions.[43] This observation has also been supported by an increase in the fragmentation yield when ECD was followed by infrared multiphoton dissociation (IRMPD).[44] In general, when applied to protein complex dissociation, the ECD-only fragmentation approach is inefficient for monomer ejection, which requires

dx.doi.org/10.1021/ac4029328 | *Anal. Chem.* XXXX, XXX, XXX−XXX

cleavages of noncovalent bonds and thus less suitable for topology of protein complexes. Consistently, while a limited number of c-ions were identified from freely available N-terminus, no C-terminal fragments could be detected.[42] It was postulated that the intact ADH complex was preserved in the gas phase by many strengthened salt bridges and ECD electrons could not access flexible internal regions in the ADH complex. In the follow up study, Zhang et al. have combined ion source CID with ECD in experiments with a Fenna-Matthews-Olson (FMO) antenna complex from green sulfur bacteria.[45] Fragment signals from one of the most flexible regions of the FMO complex were reported. However, this fragment region was also found to overlap with the flexible ECD-only fragmented C-terminal region, causing the authors to conclude that upon CID unfolding only the most flexible protein complex region would be amenable to ECD fragmentation.

Surface induced dissociation, SID, has been explored as another promising approach for collisional activation of larger protein complexes. Using a modified Waters QTOF instrument, Blackwell et al. showed SID of a heterohexamer, toyocamycin nitrile hydratase, into its constituent trimers.[46] The SID results were compared against CID data acquired with the same instrument, revealing different sets of fragments: monomers and pentamers with CID and trimers with SID. The underlining conclusion was that SID occurs on a time scale shorter than subunit unfolding and that a significant degree of secondary and tertiary structure is maintained after dissociation. While the capability of trimer ejection from the hexamer complex with SID was demonstrated, the signal-to-noise and mass resolution were poor, making peak assignment ambiguous and the follow up monomer or trimer fragmentation infeasible.

In this work, we demonstrate a novel approach for dissociation of protein complexes into the constituent monomer subunits with subsequent dissociation of monomers, whose fragment ions are then recorded at high mass resolution and mass measurement accuracy, enabling identification of precursor monomer proteoforms with high confidence.

EXPERIMENTAL SECTION

All experiments were performed with the modified Q Exactive mass spectrometer shown in Figure 1 (Thermo Fisher Scientific, Bremen, Germany) using direct ESI infusion in a nanoflow regime. Several important hardware modifications were implemented. They included (i) a novel front-end interface encompassing an orthogonal ion injection into the radio frequency (rf) field of a dual ion funnel interface; (ii) a bent flatapole with an axial electric field, which ensures efficient ion transmission at low incoming ion flux; (iii) a higher mass-to-charge (m/z) quadrupole analyzer capable of selecting precursor ion species at m/z over 20 000; (iv) reduced frequencies on the rf multipoles of the mass spectrometer, including inject and bent flatapole devices; (v) an increased gas intake into the HCD cell, which enables a pressure increase up to 2×10^{-9} mbar in the Orbitrap analyzer; and (vi) an image current preamplifier with improved linearity and a high-pass filter cutoff of 22 kHz.

Ion Funnels. A dual ion funnel instrument with orthogonal ion injection (OIDF) (Spectroglyph, Kennewick, WA) enables higher sensitivity and greater desolvation efficiency, the capabilities crucially important in native MS applications. Since its incorporation into an FTICR mass spectrometer,[47,48] the ion funnel has been commercialized, and its design was further refined by Bruker Daltonics (Billerica, MA)[49] and Agilent Technologies (Santa Clara, CA).[50] Orthogonal ion injection into the ion funnel represents another modification of the device. Gas flow through the device is one of the most crucial parameters for ion transport and focusing. Both the experiment and numerical modeling have shown that the directional subsonic gas flow would propagate into the ion funnel to a distance greater than 30 mm at an inlet capillary i.d. of 1 mm and a pressure in the device of 12 mbar. Since gas intake occurs orthogonal to the device axis in our configuration, this required an increase in the ion funnel electrode i.d. to 50 mm. The funnel spacers in the line of sight of inlet capillary were cut off, which ensured efficient removal of gas excess with a 20 m^3/h rotary pump (Edwards, U.K.). Concomitantly, larger undesolvated droplets and neutrals were also carried away, resulting in drastically reduced contamination of the downstream components of the Q Exactive mass spectrometer. The use of the confining rf field on the funnel electrodes in the region where the excess of gas is removed also decreases their contamination and facilitates stable interface operation, thereby extending instrument uptime and reducing the frequency of required cleanings. Another important characteristic of the design is complete decoupling of the gas flow and ion transport. In the coaxial ion injection scheme, gas flow into the ion funnel was found to be largely dissipated using off-axis ion injection into the device.[51] Experiments showed that under the conditions of the radially offset inlet capillary and no axial electric field, ion currents levels of >60% of that typically observed under standard operating conditions (i.e., 10 V/cm axial field) could still be detected with a mass spectrometer, mostly due to the remaining directional gas flow. In the orthogonal ion injection arrangement, no ion signals could be recorded in the absence of the axial electric field. This means that with orthogonal injection, ion residence time in the device is determined solely by the axial electric field and can be gradually adjusted to enhance droplet desolvation in the gentle rf heating environment of the device. One would emphasize that enhanced droplet desolvation is crucial for native MS applications, where nESI is performed at physiological pHs and protein complexes are introduced into the gas phase partially solvated.

To minimize capacitive load of the device on the coupled rf drive, each funnel electrode was made of a printed circuit board (PCB) with a width of the conductive trace of 2.5 mm, bringing about a total capacitance of 400 pF for the 150-mm long, 50-mm i.d. device. Additionally, to enhance funnel operation at elevated pressures of 12 mbar and above, two parallel resistor networks were employed, each coupled to the corresponding rf phase, so that an increase in the rf amplitude would not cause excessive Joule's heat dissipation on the resistors. Each funnel electrode was connected through a pair of spring loaded pins that enabled highly robust assembly and easy maintenance. The higher pressure funnel was operated at an rf amplitude of 200 V_{pp} and an rf frequency of 850 kHz. The following lower pressure funnel was offset by 5 mm relative to the higher pressure funnel axis and shaped similar to that employed in the earlier reported IMS-MS experiments.[52] The lower pressure (e.g., 2 mbar) device had a double hourglass shape to further reduce directional gas flow into the mass spectrometer and was operated at an rf amplitude of 90 V_{pp} and an rf frequency of 1 MHz. Similar to the higher pressure device, the smaller dimension (the maximum i.d. was 25 mm) ion funnel was made of PCBs with a 2.5 mm wide trace on the central aperture and

dx.doi.org/10.1021/ac4029328 | Anal. Chem. XXXX, XXX, XXX−XXX

exhibited a total capacitance of less than 300 pF. Figure 2 shows a comparison of performance of the OIDF interface against an

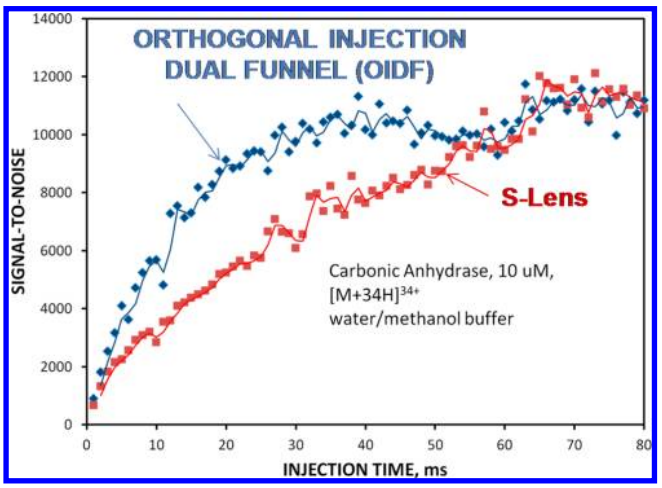

Figure 2. Signal-to-noise ratio as a function of the injection time into the C-trap for $[M + 34H]^{34+}$ ions of bovine carbonic anhydrase at 10 μM concentration. Signals were obtained with water/methanol/acetic acid buffer (49:49:2 v/v/v).

S-lens design[53] in experiments with a 10 μM solution of carbonic anhydrase electrosprayed from a water/methanol/acetic acid buffer (49:49:2 v/v/v). The data points in the graph were obtained for one of the protein charge states, $[M + 34H]^{34+}$ and represent the signal-to-noise ratio (SNR) as a function of the ion injection time into the C-trap. The general trend is the dual funnel SNR exceeds that of the S-lens by a factor of 2 at shorter injection times (<30 ms), which is consistent with the ratio in the inlet capillary areas (1 mm i.d for the dual funnel and 0.6 mm i.d. for the S lens). At longer injection times, the C-trap gets filled up to its capacity resulting in similar SNRs for both interfaces. It is worth noting that ion transport through the S-lens is governed by the gas flow, while in the dual funnel with orthogonal injection ions traverse the interface region only under the influence of an adjustable electric field.

Quadrupole rf Drive and Mass Spectrometer Modifications. The standard Q Exactive quadrupole rf drive has been modified by rewinding the output coils and increasing the resonance contour inductance by a factor of 9. This resulted in a decrease of the resonant rf frequency to 284 kHz and enabled higher m/z selection up to m/z 20 000. Concurrently, new software has been developed to ensure reliable m/z calibration and isolation at a mass resolution of greater than 70 in the m/z

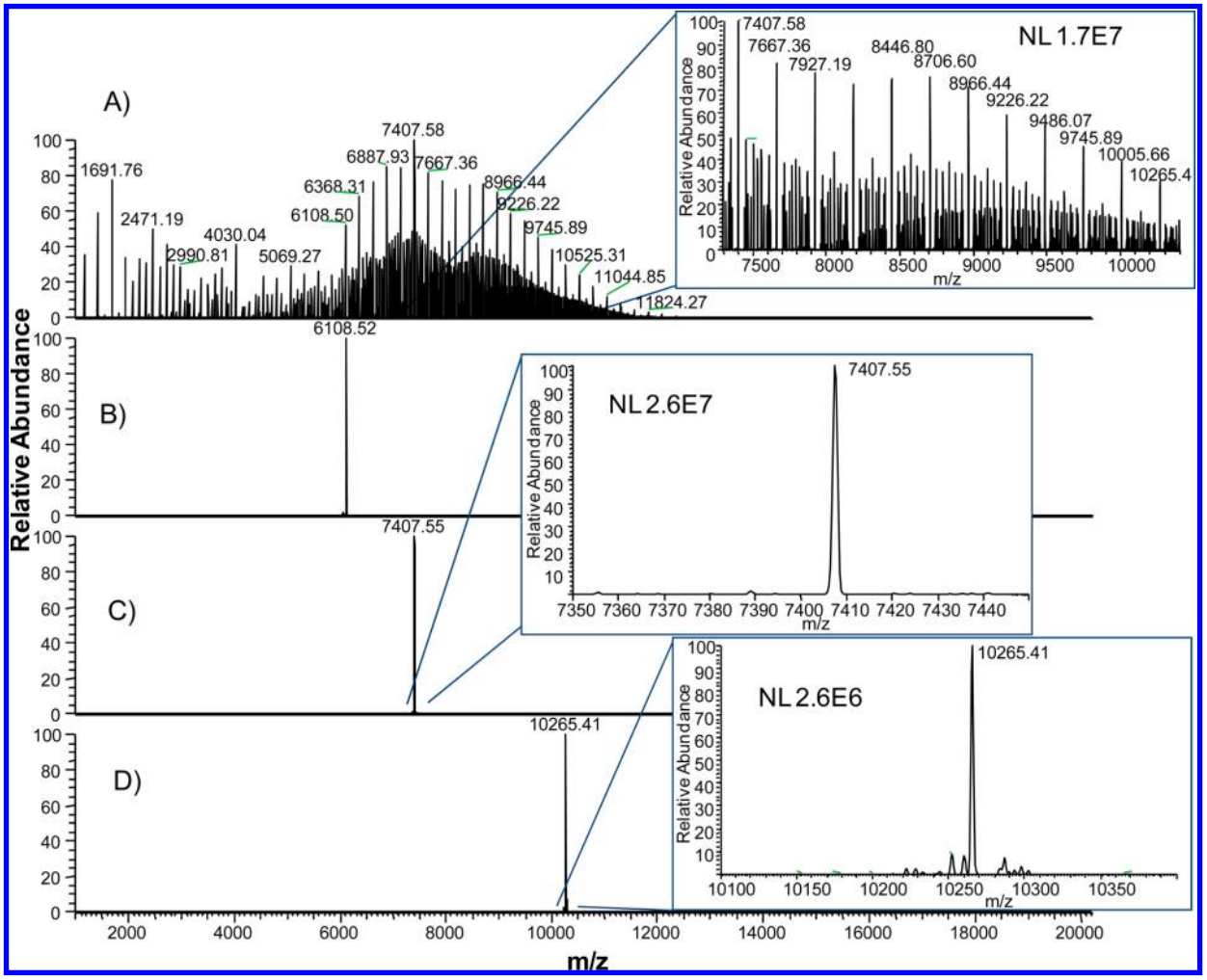

Figure 3. Full MS and quadrupole-selection mass spectra of aqueous solution of CsI at a concentration of 60 mg/mL obtained with the modified Q Exactive MS. Ion trapping was performed in the C-trap.

dx.doi.org/10.1021/ac4029328 | Anal. Chem. XXXX, XXX, XXX–XXX

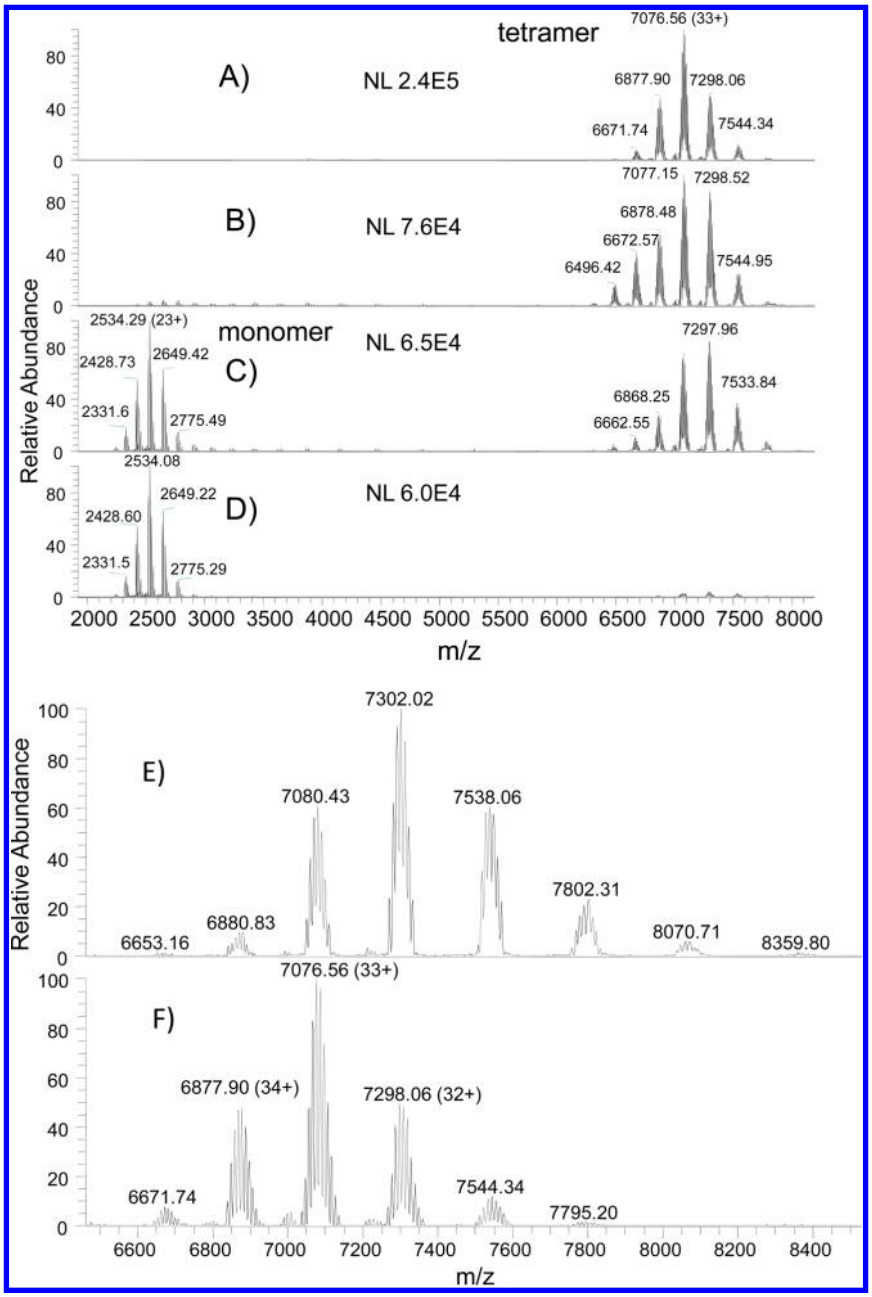

Figure 4. Mass spectra of a native 10 μM pyruvate kinase sample obtained under different ion trapping and activation conditions. Each spectrum is an average of 100 microscans. (A) HCD collision energy of 100 V; (B) HCD collision energy of 120 V; (C) HCD collision energy of 200 V; (D) HCD collision energy of 200 and 10 V activation after the dual funnel interface; (E) S-lens, 30 V collisional activation prior to inject flatapole; 200 V activation in the HCD cell; (F) Dual-funnel interface with orthogonal ion injection: no activation prior to inject flatapole; 100 V activation in the HCD cell.

range exceeding 10 000 Th. We have examined quadrupole isolation efficiency in a higher m/z range by varying both a and q Mathieu's parameters in close proximity to the apex of quadrupole stability diagram for a given m/z species. It was found that the isolation window has relatively wide roll-off edges (e.g., signal amplitude drops 50% within 5 V_{pp} range at the stability diagram apex, corresponding to $q = 0.7$, $a = 0.236$), presumably due to fringing rf fields typically observed for the circular solid rod geometry (no preimposed filters). Figure 3 shows signals obtained with a 60 mg/mL aqueous solution of CsI. The top panel depicts a full MS spectrum, whereas the lower panels show spectra obtained using the rf/dc quadrupole filter. The insets illustrate narrow m/z ranges corresponding to the selected CsI cluster ions. As evident from Figure 3, the modified quadrupole rf drive is capable of selecting relatively narrow m/z regions ($\Delta m/z$ < 100 Th) in the m/z region exceeding 10 000 Th at only 20−30% ion transmission losses.

To enhance ion transmission in the m/z range exceeding 3 000 Th, the rf frequency of inject and bent flatapoles was reduced to 2.6 MHz. Also, a 50 μm i.d. gas restrictor line coupling nitrogen pressure regulator and HCD cell enabled a user-defined pressure adjustment in the HCD cell above 10^{-3}–10^{-2} mbar.

Sample Preparation and Ionization. Protein samples in lyophilized form, such as pyruvate kinase (KPYM_RABIT; Uniprot ID, P11974; MW 58 kDa as monomer), phosphorylase

dx.doi.org/10.1021/ac4029328 | Anal. Chem. XXXX, XXX, XXX−XXX

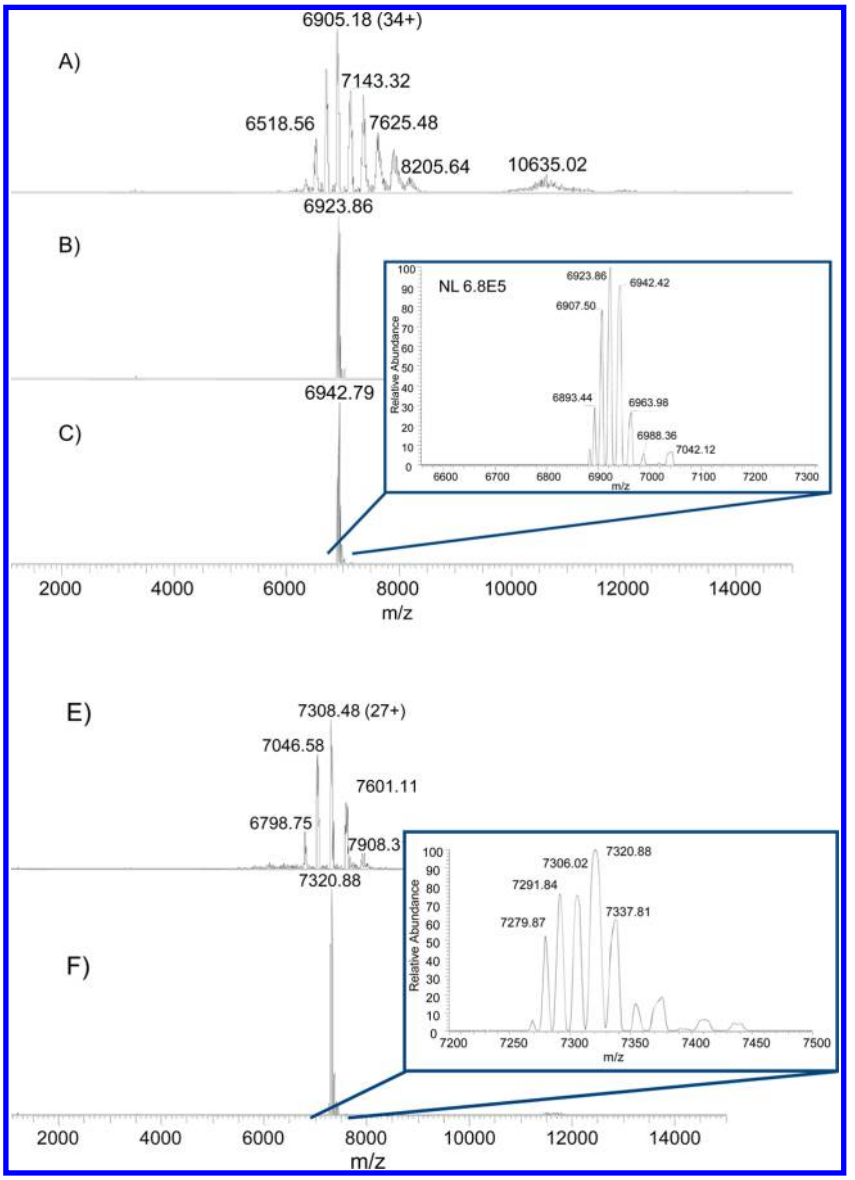

Figure 5. (A–C) Mass spectra of native 10 μM pyruvate kinase and (D,E) 10 μM phosphorylase b samples obtained under different ion trapping and preselection conditions. Ion trapping on the C-trap was performed at an activation energy of 2 V. (A) Full MS spectrum of pyruvate kinase. The molecular ions of intact protein complex was accumulated in the C-trap; (B) pyruvate kinase selective accumulation in the C-trap; (C) pyruvate kinase selective accumulation in the HCD cell at an activation energy of 1 V; (D) full MS spectrum of phosphorylase B accumulated in the C-trap; (E) phosphorylase B selective accumulation in the C-trap. Each spectrum is an average of three microscans.

B (KPBB_RABIT; Uniprot ID, P00489; MW 97 kDa as monomer), were purchased from Sigma Aldrich Chemie (Munich, Germany) and purified using buffer exchange and centrifugation with Micro Bio Rad Spin 6 columns (Bio-Rad Laboratories, Hercules, CA). GroEL (MW 801 kDa) was expressed recombinantly in *E. coli* as previously described.[54] All samples were reconstituted in 100 mM ammonium acetate buffer and diluted to a concentration of 10 μM.

Sample ionization was performed in the nESI regime at a flow rate of ~1–2 μL/h. Both gold-coated glass tips of 2–4 μm i.d. (Thermo Fisher Scientific, Bremen, Germany) and a Triversa Nanomate (Advion Biosciences, Ithaca, NY) were employed for generating nESI signals. In the latter setup, a microarray chip with 6 μm i.d. nESI nozzles was used. Upon ionization, nESI droplets were captured by a 1-mm i.d. 7 cm-long stainless capillary maintained at a temperature of 140 °C and introduced orthogonally into the higher pressure ion funnel.

Instrument Control and Data Processing Software. Instrument control and raw data acquisition were accomplished using Exactive Plus 2.2 software (with developer access enabled). Raw data were then visualized and processed with the Xcalibur 2.2 package, which encompasses the Xtract algorithm for extracting monoisotopic signals. Deconvolution of m/z spectra of the monomer subunits was conducted with Protein Deconvolution 2.0 software. Processing of fragmentation mass spectra as well as determination of cleavage sites, post-translational modifications, and fragment assignments were carried out with ProsightPC 3.0 software (all of the above software packages are commercially available from Thermo Fisher Scientific). Molecular weight measurements of protein complexes were performed by taking the apexes of all m/z peaks in a charge-state distribution and calculating the

dx.doi.org/10.1021/ac4029328 | *Anal. Chem.* XXXX, XXX, XXX–XXX

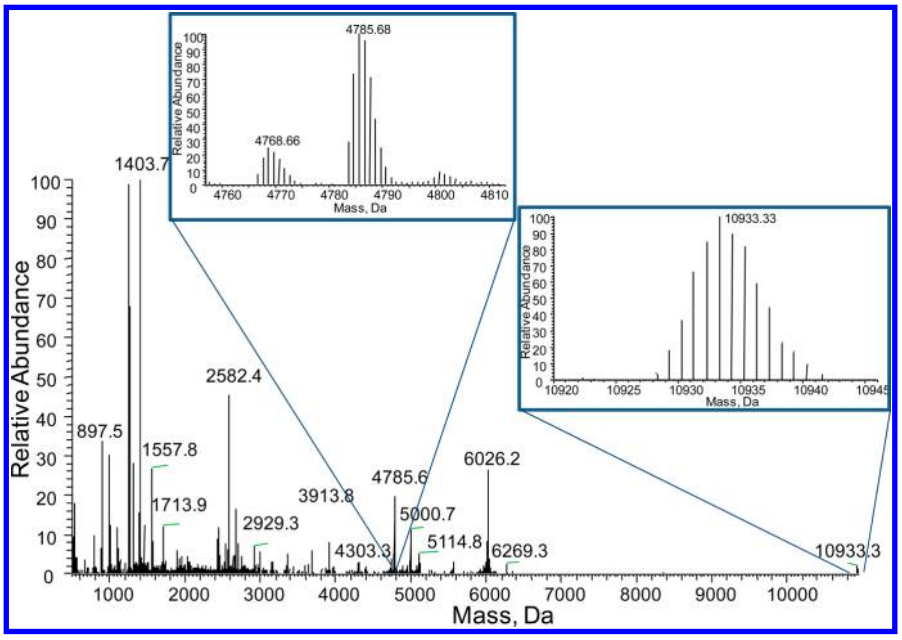

Figure 6. Fragmentation mass spectrum of pyruvate kinase monomer ejected from the intact tetramer complex. Pressure in the HCD cell was 8×10^{-10} mbar. The inset demonstrates fragment ion matches against the pyruvate kinase sequence at mass measurement accuracy better than 15 ppm.

charge state manually. The molecular weights were then calculated from each charge state peak, and the average and standard deviation were reported.

RESULTS AND DISCUSSION

Figure 4A–F shows the evolution of signals of a noncovalent tetramer complex of pyruvate kinase under different experimental conditions. The collision energy in the higher collision energy dissociation (HCD) cell was adjusted by applying a corresponding bias to the HCD cell rods relative to the HCD entrance lens. During ion trapping in the HCD cell, an axial electric field gradient of 3 V/cm in the direction opposite to the initial velocity of the ions was applied to ensure ion accumulation in close proximity to the HCD cell entrance lens. An increase in the collision energy resulted in dissociation of the protein complex and a release of highly charged monomer species, as shown in Figure 4A–D. An inset demonstrates charge state signals of the tetramer complex at different degrees of collisional activation, revealing well-resolved forms of the complex. An additional collisional activation in the region between the dual funnel and inject flatapole gave rise to nearly complete dissociation of the tetramer complex into the constituent monomers. Figure 4E,F shows the comparison of signals of the pyruvate kinase tetramer complex obtained with an S-lens and the dual funnel interfaces using the same mass spectrometer. While the S-lens arrangement required 30 V "in-source" activation (between the S-lens exit electrode and inject flatapole) and the maximum HCD collision energy to obtain partially resolved signals of the complex, the dual funnel interface enabled detection of the intact tetramer complex without "in-source" activation and at one-half of the HCD collision energy required for the S-lens design. Additionally, close examination of the tetramer charge state signals revealed higher mass resolution of the various signals of the complex, which were acquired with the dual funnel interface. We attribute these significant differences in the required degrees of collisional activation after the two interfaces to difference in their desolvation efficiencies for partially solvated pyruvate kinase tetramer complexes. Further experimental evidence of the improved desolvation with the OIDF interface as compared to the S-lens is shown in Figure S1A,B in the Supporting Information, which provides back-to-back comparison of GroEL native MS spectra acquired at low collision energy (an HCD bias of 1 V) with both arrangements. As seen in Figure S1C,D in the Supporting Information, the S-lens desolvation is improved by increasing the HCD bias to ~100 V, which somewhat limits the amount of energy to be used for fragmentation of the ejected monomer subunits to backbone fragments.

In the Supporting Information, Figure S2 shows the raw m/z and deconvoluted mass spectra of the pyruvate kinase monomer signals are shown in Figure 4C,D. With the resolution provided by this approach, interesting biochemistry may be seen even with standard proteins. Pyruvate kinase has four isozymes in mammals that are encoded by two genes: L for liver, R for red blood cells, and M1 and M2 for muscle. The monomers are known to have possible acetylations at seven sites and phosphorylations at five sites. Furthermore, pyruvate kinase reversibly associates to form a homotetramer with allosteric regulators such as 2,5-anhydro-D-glucitol, 1,6 bisphosphate (GBP). In Figure S-1 in the Supporting Information, the unmodified monomer peak was matched to the theoretical mass within 15 ppm: the initiation Met residue was removed and the N-terminal Ser was found to be acetylated. The 324 ± 0.6 Da mass difference observed for the modified forms seen matches that of GBP (average mass, 324 Da). It is apparent that the GBP adducts are stable under collisional activation. To our knowledge, this is the first measurement of GBP stoichiometry for tetrameric pyruvate kinase.

Figure 5A–E depicts mass spectra of the native pyruvate kinase and phosporylase B complexes using the dual funnel interface in conjunction with quadrupole mass preselection. Importantly, large molecular ions of the intact protein complexes were found to be efficiently trapped in both the C-trap and HCD cell at low collision energies (<5 V) and then

dx.doi.org/10.1021/ac4029328 | Anal. Chem. XXXX, XXX, XXX–XXX

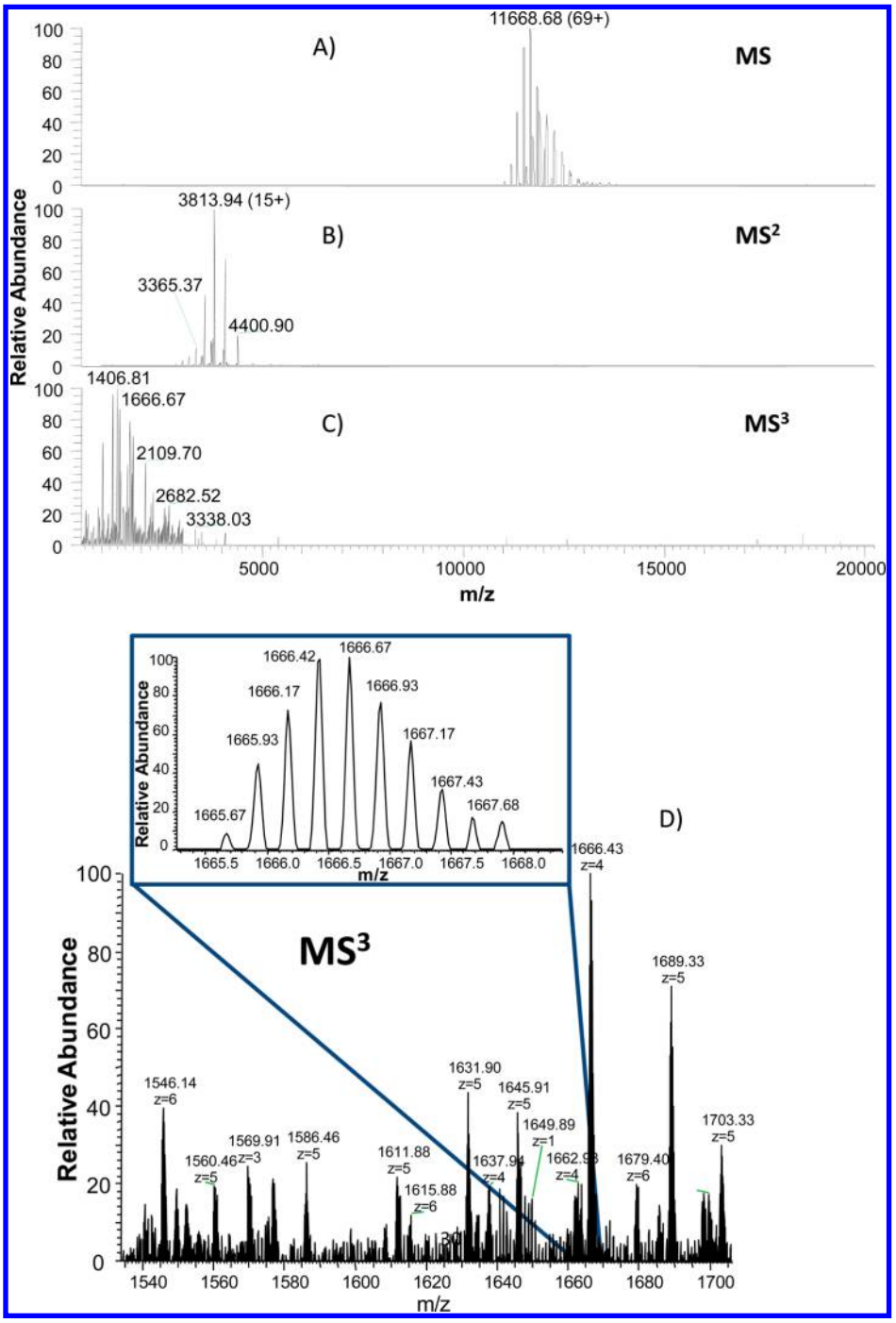

Figure 7. GroEL mass spectra acquired under the following conditions: (A) signal obtained by trapping an intact 14-mer GroEL complex in the C-trap; (B) signal of the GroEL monomer subunit obtained upon collisional activation between the funnel exit electrode and inject flatapole. The GroEL monomer ions were accumulated in the C-trap; (C) subunit backbone-level spectrum upon 200 V collisional activation in the HCD cell; (D) narrow region of the MS^3 mass spectrum with charge state annotations. The inset shows the signal of one of the GroEL fragment ions (b63) identified at a mass measurement accuracy of 2.3 ppm.

detected with the Orbitrap mass analyzer at a signal-to-noise ratio of >1000. The insets demonstrate signals of the quadrupole-preselected pyruvate kinase and phosphorylase b intact protein complexes. Our attempts to acquire signals with the S-lens interface under the identical conditions were unsuccessful, as no discernible mass spectral peaks could be observed even with spectral averaging. This observation also consistently points to the fact that the dual funnel interface with orthogonal ion injection facilitates improved desolvation of large protein complexes.

To enable a two-step fragmentation pathway (or pseudo-MS^3), the protein complex of interest needs to be significantly desolvated immediately after the front-end interface. As demonstrated in Figures 4 and 5, the dual funnel interface with orthogonal ion injection is capable of providing such a degree of desolvation under the optimized conditions. Our strategy for achieving the unprecedented level of character-

dx.doi.org/10.1021/ac4029328 | Anal. Chem. XXXX, XXX, XXX−XXX

ization of stoichiometry and composition of monomers ejected from larger protein complexes has been as follows. Upon exiting the dual funnel, an intact protein complex was dissociated in the region between the funnel exit electrode and the inject flatapole. The released highly charged monomer ions (MS^2) were then selected with the quadrupole mass analyzer and introduced into the HCD cell for fragmentation. Upon fragment ion transfer into the C-trap and Orbitrap detection, high resolution and high mass accuracy fragment signals were acquired and spectral features were assigned and identified and then mapped back to the intact protein monomer and, concomitantly, to the intact protein complex.

Figure 6 shows subunit backbone fragmentation mass spectrum obtained in the pseudo-MS^3 experiment with tetramer complexes of pyruvate kinase. The extracted monoisotopic signals were processed by ProsightPC software and correlated against the known pyruvate kinase protein sequence. The insets to Figure 6 show two subunit backbone fragments identified at mass measurement accuracies of 11.6 ppm (y45, 4898.72 Da) and 3.3 ppm (b100, 10927.30 Da). A total of 63 unique subunit backbone fragments were identified at a mass resolution of 70 000, corresponding to 40 y- and 23 b-multiply charged fragment ions (PDE score, 11.5; expectation value, 3×10^{-13}). Interestingly, many of the identified subunit backbone fragments were found to have molecular masses over 3000 Da, typically beyond the mass range of conventional bottom-up proteomics, while a selected number of fragment ions (y45−y75 and b43−b100) had molecular masses exceeding 5 000 Da. In the Supporting Information, Tables S1 and S2 show all the identified subunit backbone fragments at mass measurement accuracy better than 15 ppm and a backbone cleavage map of the pyruvate kinase sequence, respectively. Close examination of the sequence ladder of y fragments reveals that the sequential backbone cleavages terminate at the Cys residue (position y58). A similar pattern is also observed for the consecutive cleavages at N-terminus, which interrupt at another Cys residue (position b30). Though no disulfides are reported for pyruvate kinase, it is possible that some are present from oxidation in ESI and the observed termination of backbone cleavages could be related to the known CID inefficiency to rupture disulfide bonds.[55] Further investigation would be needed to accurately determine locations of disulfide bonds in pyruvate kinase and probe them with alternative approaches, such as electron transfer dissociation (ETD).[56]

Figure 7A−D shows the complete two-step fragmentation pathway from the native protein complex to the spectrum of subunit backbone fragments for the GroEL (MW 801 kDa) sample nanoelectrosprayed from a 100 mM ammonium acetate buffer. The top panel (A) illustrates the intact 14-mer GroEL complex trapped in the C-trap under gentle activation conditions: no axial electric field between the funnel exit electrode and inject flatapole, and no collisional desolvation during ion injection into the C-trap. The middle panel (B) depicts the signal obtained upon ion activation between the funnel exit electrode and inject flatapole using an axial field gradient of 30 V/mm. As evidenced from the mass spectrum, the highly charged monomer ions have been released upon GroEL complex dissociation to be referred to as the pseudo-MS^2 experiment. The bottom panel (C) shows the subunit backbone-level spectrum obtained after isolation of the GroEL most abundant charge states in the selection quadrupole, to be referred to as the pseudo-MS^3 spectrum. The MS^3 spectrum has been obtained at a collision energy of 200 V, which is currently the maximum voltage available for ion activation in the HCD cell. The inset demonstrates a narrow m/z region of the MS^3 spectrum with fully resolved multiply charged fragment signals acquired at a mass resolution of 70 000. Similarly to the pyruvate kinase processing pipeline, Tables S3 and S4 (in the Supporting Information) report the high confidence matches against the known GroEL protein sequence using a mass measurement accuracy better than 15 ppm and the cleavage map of the GroEL monomer subunit, respectively. As a result, 6 y and 49 b fragment ions have been identified that enables unambiguous identification of the GroEL monomer (PDE score, 10.9; expectation value, 4×10^{-23}). Our analysis of the protein sequence indicates that deeper fragmentation (i.e., greater protein coverage) could be obtained by reducing disulfide bonds of the protein.

The presented experimental evidence of the successful MS^3 fragmentation pathway of large protein complexes is an important advance for characterizing native protein complexes and their constituent subunits with tandem MS. Herewith, we would summarize our observations on implementation of the two-step fragmentation pathway of the protein complexes electrosprayed from aqueous buffers at physiological pH values and detected with a high resolution Orbitrap MS.

One of the most important characteristics for the two-step sequencing of native protein complexes is efficient desolvation. Once a protein complex is ionized from a neutral pH buffer and introduced into a mass spectrometer partially solvated, the solvent and salts can only be "shaken off" in the collision chamber of the instrument. We have obtained the experimental evidence that if a solvated intact protein complex is carried through the front-end interface with a directional gas flow, desolvation is inefficient, placing most of the burden for solvent removal onto the collision cell. While the clean up and restructuring of the native protein complex in the collision cell is feasible,[38] it requires a significant degree of collisional activation. Because of practical design constraints, this initial activation limits the amount of energy which could be then effectively used for ejecting protein subunits from a complex and for subsequent fragmentation of the released subunits. In addition, collisional activation at higher energy in a single collision cell would not permit isolation and selective activation of structurally different subunits of a heteromeric protein complex. As a result, even if successfully implemented, this single-step desolvation/fragmentation pathway would result in highly congested mass spectra that could be difficult, if not impossible, to interpret. When used in conjunction with high-resolution FTICR MS instruments, such as an instrument utilizing an Orbitrap analyzer, acquisition of fragmentation spectra from the intact protein complexes in the single-step dissociation/fragmentation pathway would simply be impossible, as trapping larger protein complexes requires elevated pressures ($>10^{-2}$ mbar) in the HCD cell that is incompatible with high vacuum requirement ($<7 \times 10^{-10}$ mbar) for high-resolution detection of subunit backbone fragment signals. Therefore, high-resolution high-mass-accuracy detection of fragment ions originating from an intact protein complex with the Orbitrap analyzer would only be feasible at low pressures ($<7 \times 10^{-3}$ mbar) in the HCD cell. Important ramification of this requirement is a two-step fragmentation process, in which two ion activation regions should ideally be separated by a mass selection device. It is imperative, however, that the native protein complexes are largely desolvated prior to the first activation step, otherwise most of the activation energy

dx.doi.org/10.1021/ac4029328 | Anal. Chem. XXXX, XXX, XXX−XXX

would be deposited to solvent removal rather than complex dissociation.

Whereas our work represents a major advance in improving desolvation efficiency of the front-end interface, further enhancements are still needed. For example, ion accumulation in the C-trap and HCD cell at low collision energy (~1 V) and Orbitrap detection with the dual funnel interface was found to yield high-quality mass spectra with an SNR >1000. However, mass spectral assignment of the intact protein complex peaks remains to be challenging at low collision energies (<5 V). Detailed examination of the mass spectra of the intact pyruvate kinase tetramer in Figures 4A–C and 5A–C shows that the maximum signal for the 34+ charge state has shifted from m/z 6877.9 to m/z 6905.2 at collisonal activations of 120 and 1 V in the HCD cell, respectively. The reported difference in the m/z peak position corresponds to a shift of 929 Da in the neutral mass domain. This means that, though drastically improved, desolvation of intact protein complexes with the dual interface is still incomplete and accurate assignment of intact protein complex peaks just based on molecular mass measurement would be ambiguous and dependent upon the degree of intact complex desolvation. Therefore, deeper fragmentation of intact protein complexes for accurate determination of their mass and composition, i.e., MS^3 activation implemented in this work, and further improvements in the desolvation efficiency will be crucially important in future native MS developments.

Another important observation is related to the fragmentation efficiency of subunits of native protein complexes. Our work has shown that multistage fragmentation of an intact protein complex followed by high-resolution, high-accuracy detection of backbone fragmentation products is feasible in a two-step fragmentation pathway with quadrupole selection of the released highly charged subunits. However, like top down MS experiments in general, fragmentation efficiency toward the middle of protein monomer sequences was found to be sparse from either insufficient activation energy or disulfide bonding. One approach for further increasing fragmentation yield would be to employ alternative fragmentation approaches such as ETD, UVPD,[57] or higher energy SID in the HCD cell. These techniques can be performed at low pressure in the HCD cell and are expected to generate a complementary set of fragments to those previously observed with HCD.

CONCLUSIONS

In this work, a novel two-step fragmentation methodology enabled sequence analysis of large protein complexes ionized from buffers at physiological pH. The approach incorporates highly efficient desolvation of protein complexes in the front-end interface, a release of monomer subunits during collisional activation immediately downstream of the interface (MS^2), preselection of the monomer species of interest followed by higher energy collisional activation (MS^3), which produced a set of multiply charged backbone fragments characterizing the protein monomers. All experiments were performed using high-resolution and high-accuracy Orbitrap MS, resulting in high confidence identifications of ejected monomers. The identified fragments were mapped back to the protein sequence, and fragmentation map and sequence coverage were reported. The developed approach represents a significant advance in the application of native MS and is expected to be widely embraced for characterization of stoichiometry and composition of heteromeric intact protein complexes.

ASSOCIATED CONTENT

Supporting Information

Additional information as noted in text. This material is available free of charge via the Internet at http://pubs.acs.org.

AUTHOR INFORMATION

Corresponding Author

*E-mail: n-kelleher@northwestern.edu.

Present Address

[§]M.E.B.: Spectroglyph LLC, Kennewick, WA 99338.

Notes

The authors declare the following competing financial interest(s): Mikhail Belov, Eugen Damoc, Eduard Denisov, Stevan Horning and Alexander Makarov are employees of Thermo Fisher Scientific.

ACKNOWLEDGMENTS

The authors are grateful to Prof. Albert Heck and his group at Utrecht University, The Netherlands, for purifying the GroEL complexes. M.E.B. acknowledges Dr. Jan-Peter Hauschild's assistance in enabling quadrupole mass selection in the extended m/z range and Aron Fenton for helpful discussions regarding pyruvate kinase. The work was made possible by generous support from Northwestern University and the W.M. Keck Foundation.

REFERENCES

(1) Robinson, C. V.; Sali, A.; Baumeister, T. L. *Nature* **2007**, *450*, 973–982.
(2) Charbonnier, S.; Gallego, O.; Gavin, A. C. *Biotechnol. Annu. Rev.* **2008**, *14*, 1–28.
(3) Bader, S.; Kuhner, S.; Gavin, A. C. *FEBS Lett.* **2008**, *582*, 1220–1224.
(4) Ban, N.; Egelman, E. H. *Curr. Opin. Struct. Biol.* **2010**, *20*, 207–209.
(5) Ganem, B.; Li, Y. T.; Henion, J. D. *J. Am. Chem. Soc.* **1991**, *113*, 6294–6296.
(6) Katta, V.; Chait, B. T. *J. Am. Chem. Soc.* **1991**, *113*, 8534–8535.
(7) Loo, J. A. *Mass Spectrom. Rev.* **1997**, *16*, 1–13.
(8) van der Heuvel, R. H.; Heck, A. J. *Curr. Opin. Chem. Biol.* **2004**, *8*, 519–526.
(9) Sharon, M.; Robinson, C. V. *Annu. Rev. Biochem.* **2007**, *76*, 167–193.
(10) Kocher, T.; Superti-Furga, G. *Nat. Methods* **2007**, *4*, 807–815.
(11) Heck, A. J. *Nat. Methods* **2008**, *5*, 927–933.
(12) Benesch, J. L.; Ruotolo, B. T. *Curr. Opin. Struct. Biol.* **2011**, *21*, 641–649.
(13) Benesch, J. L.; Ruotolo, B. T.; Sobott, F.; Wildgoose, J.; Gilbert, A.; Bateman, R.; Robinson, C. V. *Anal. Chem.* **2009**, *82*, 1270–1274.
(14) Van den Heuvel, R. H. H.; van Dujin, E.; Mazon, H.; Synowsky, S. A.; Lorenzen, K.; Versluis, C.; Brouns, S. J. J.; Langridge, D.; van der Ooost, J.; Hoyes, J.; Heck, A. J. R. *Anal. Chem.* **2006**, *78*, 7473–7483.
(15) Wimberley, B. T.; Brodersen, D. E.; Clemons, W. M., Jr.; Morgan-Warren, R. J.; Carter, A. P.; Vonrhein, C.; Hartschk, T.; Ramakrishnan, V. *Nature* **2000**, *407*, 327–339.
(16) Ban, N.; Nissen, P.; Hansen, J.; Moore, P. B.; Steitz, T. A. *Science* **2000**, *289*, 905–920.
(17) Zuiderweg, E. R. P. *Biochemistry* **2002**, *41* (1), 1–7.
(18) Takeuchi, K.; Wagner, G. *Curr. Opin. Struct. Biol.* **2006**, *16*, 109–117.
(19) Loquet, A.; Laage, S.; Gardiennet, C.; Elena, B.; Emsley, L.; Bockmann, A.; Lesage, A. *J. Am. Chem. Soc.* **2008**, *13*, 10625–10632.
(20) Grishaev, A.; Wu, J.; Trewhella, J.; Bax, A. *J. Am. Chem. Soc.* **2005**, *127*, 16621–16628.

(21) Mertens, H. D.; Svergun, D. J. *J. Struct. Biol.* **2010**, *172*, 128−141.
(22) Poliakov, A.; van Dujin, E.; Lander, G.; Fu, C. Y.; Johnson, J. E.; Prevelige, P. E., Jr.; Heck, A. J. *J. Struct. Biol.* **2007**, *157*, 371−383.
(23) Wilm, M.; Mann, M. *Anal. Chem.* **1996**, *68*, 1−8.
(24) Breuker, K.; McLafferty, F. W. *Proc. Natl. Acad. Sci. U.S.A.* **2008**, *105*, 18245−18152.
(25) Ruotolo, B. T.; Giles, K.; Campuzano, I.; Sandercock, A. M.; Bateman, R. H.; Robinson, C. V. *Science* **2005**, *310*, 1658−1661.
(26) Ruotolo, B. T.; Benesch, J. L. P.; Sandercock, A. M.; Hyung, S.-J.; Robinson, C. V. *Nat. Protoc.* **2008**, *3*, 1139−1152.
(27) Uetrecht, C.; Versluis, C.; Watts, N. R.; Wingfeld, P. T.; Steven, A. C.; Heck, A. J. *Angew. Chem., Int. Ed.* **2008**, *47*, 6247−6251.
(28) van Duijn, E.; Barendregt, A.; Synowsky, S.; Vesluis, C.; Heck, A. J. *J. Am. Chem. Soc.* **2009**, *131*, 1452−1459.
(29) Giles, K.; Pringle, S. D.; Worthington, K. R.; Little, D.; Wildgoose, J. L.; Bateman, R. H. *Rapid Commun. Mass Spectrom.* **2004**, *18*, 2401−2414.
(30) Pringle, S. D.; Giles, S.; Wildgoose, J. L.; Williams, J. P.; Slade, S. E.; Thlassinos, K.; Bateman, R. H.; Bowers, M. T.; Scrivens, J. H. *Int. J. Mass Spectrom.* **2007**, *261*, 1−12.
(31) Ueterecht, C.; Rose, R. J.; van Duijin, E.; Lorenzen, K.; Heck, A. J. R. *Chem. Soc. Rev.* **2009**, *39*, 1633−1655.
(32) Ueterecht, C.; Versluis, C.; Watts, N. R.; Roos, W. H.; Wuite, G. J. L.; Wingfeld, P. T.; Steven, A. C.; Heck, A. J. R. *Proc. Natl. Acad. Sci. U.S.A.* **2008**, *105*, 9216−9220.
(33) Barrera, N.; Di Bartolo, N.; Booth, P. J.; Robinson, C. V. *Science* **2008**, *321*, 243−246.
(34) Rose, R. J.; Damoc, E.; Denisov, E.; Makarov, A. A.; Heck, A. J. R. *Nat. Methods* **2012**, *9*, 1084−1086.
(35) Kellie, J. F.; Catherman, A. D.; Durbin, K. R.; Tran, J. C.; Tipton, J. D.; Norris, J. L.; Witkowski, C. E.; Thomas, P. M.; Kelleher, N. L. *Anal. Chem.* **2012**, *84*, 209−215.
(36) Jennings, K. R. *Int. J. Mass Spectrom.* **2000**, *200*, 479−493.
(37) Shukla, A. K.; Futrell, J. H. *J. Mass Spectrom.* **2000**, *35*, 1069−1090.
(38) Benesch, J. L. P. *J. Am. Soc. Mass Spectrom.* **2009**, *20*, 341−348.
(39) van Duijn, E.; Simmons, D. A.; van den Heuvel, R. H.; Bakkes, P. J.; van Heerikhuizen, H.; Heeren, R. M.; Robinson, C. V.; van der Vies, S. M.; Heck, A. J. *J. Am. Chem. Soc.* **2006**, *128*, 4694−4702.
(40) Lomeli, S. H.; Yin, S.; Ogorzalek Loo, R. R.; Loo, J. A. *J. Am. Soc. Mass Spectrom.* **2009**, *20*, 593−596.
(41) van Duijn, E. *J. Am. Soc. Mass Spectrom.* **2010**, *21*, 971−978.
(42) Zhang, H.; Cui, W.; Wen, J.; Blankenship, R. E.; Gross, M. L. *J. Am. Soc. Mass Spectrom.* **2010**, *21*, 1966−1968.
(43) Zubarev, R. A. *Curr. Opin. Biotechnol.* **2004**, *15*, 12−16.
(44) Breuker, K.; Oh, H.; Lin, C.; Carpenter, B. K.; McLafferty, F. W. *Proc. Natl. Acad. Sci. U.S.A.* **2004**, *101*, 14011−14016.
(45) Zhang, H.; Cui, W.; Gross, M. L.; Blankenship, R. E. *FEBS Lett.* **2013**, *587*, 1012−1020.
(46) Blackwell, A. E.; Dodds, E. D.; Bandarian, V.; Wysocki, V. H. *Anal. Chem.* **2011**, *83*, 2862−2864.
(47) Belov, M. E.; Gorshkov, M. V.; Anderson, G. A.; Udseth, H. R.; Smith, R. D. *Anal. Chem.* **2000**, *72*, 2271−2279.
(48) Belov, M. E.; Gorshkov, M. V.; Udseth, H. R.; Anderson, G. A.; Tolmachev, A. V.; Prior, D. C.; Harkewicz, R.; Smith, R. D. *J. Am. Soc. Mass Spectrom.* **2000**, *11*, 19−23.
(49) Kim, T.; Park, M. *Ion guide for mass spectrometers*. U.S. Patent 8,222,597, July 17, 2012.
(50) Mordehai, A.; Werlich, M. *Ion funnel for mass spectrometry*. U.S. Patent 8,324,565, December 4, 2012.
(51) Belov, M. E.; Zhang, R.; Anderson, G. A.; Strittmatter, E.; Prior, D. C.; Tang, K.; Smith, R. D. *Anal. Chem.* **2003**, *75*, 4195−4205.
(52) Belov, M. E.; Clowers, B. H.; Prior, D. C.; Danielson, W. F.; Liyu, A. V.; Petritis, B. O.; Smith, R. D. *Anal. Chem.* **2008**, *80*, 5873−5883.
(53) Olsen, J. V.; Schwartz, J. C.; Griep-Raming, J.; Nielsen, M. L.; Damoc, E.; Denisov, E.; Lange, O.; Remes, P.; Taylor, D.; Splendore, M.; Wouters, E. R.; Senko, M.; Makarov, A.; Mann, M.; Horning, S. *Mol. Cell. Proteomics* **2009**, *8*, 2759−2769.
(54) Quaite-Randall, E.; Joachimiak, A. *Methods Mol. Biol.* **2000**, *140*, 29−39.
(55) Han, X.; Jin, M.; Breuker, K.; McLafferty, F. W. *Science* **2006**, *314*, 109−112.
(56) Syka, J. E. P.; Coon, J. J.; Schroeder, M. J.; Shabanowitz, J.; Hunt, D. F. *Proc. Natl. Acad. Sci. U.S.A.* **2004**, *101*, 9528−9533.
(57) Shaw, J. B.; Li, W.; Holden, D. D.; Zhang, Y.; Griep-Raming, J.; Fellers, R. T.; Early, B. P.; Thomas, P. M.; Kelleher, N. L.; Brodbelt, J. S. *J. Am. Chem. Soc.* **2013**, *135*, 12646−12651.